34th AIAA Fluid Dynamics Conference and Exhibit
28 June - 1 July 2004, Portland, Oregon

AIAA 2004-2719

An Analysis of Pitot and Static Pressure Measurements in an Unsteady Supersonic Flow

Kathleen M. Tacina * Rene Fernandez † John W. Slater†

Stefanie M. Moody ‡

National Aeronautics and Space Administration, Glenn Research Center, Cleveland, OH 44135

An unsteady supersonic ejector with subsonic secondary flow was investigated experimentally. To understand the wave physics of the pulsed ejector, dynamic pressure measurements were examined for primary flow Mach numbers of 3.7 and 5, secondary flow Mach number of 0.3, frequencies of 30 to 120 Hz, and a duty cycle (defined as the pulse duration to total cycle duration) of 8%. It was found that the pressure signals were complex, with short wavelength pressure "pulses" superimposed on pulses with longer wavelength. Spectral, wavelet, and Hilbert-Huang transform analyses were performed. The Hilbert-Huang transform analysis proved the most useful, and will be in used in the method being developed to automate the analysis of the pressure measurements.

I. Introduction

In the past, most aerospace propulsion applications have involved processes that are steady, quasi-steady , and/or subsonic. However, alternative engine cycles such as the pulse detonation engine produce flow that is both supersonic and unsteady. Unsteady supersonic flow requires data analysis techniques not required for either steady (supersonic or subsonic) flow or unsteady subsonic flow.

This paper describes the method developed to study the wave physics in a pulsed ejector experiment with mixed supersonic and subsonic flow. In this experiment, a small supersonic nozzle emptying into a wind tunnel run at low subsonic speeds was used to simulate a pulse detonation engine emptying into an ejector. The nozzle provided the high speed of a pulse detonation engine exhaust (the primary flow Mach number, $M = 3.7$ to 5), while the wind tunnel provided a low speed secondary flow ($M = 0.2$ to 0.4).

The purpose of this pulsed ejector experiment is to (1) determine the thrust augmentation as a function of pulse rate, pulse strength, pulse duty cycle, primary flow gas, primary flow Mach number, and secondary flow Mach number and (2) to study the wave physics and vortex structure of the pulsed ejector. A 17-probe cross-shaped pitot rake was used in conjunction with static pressure taps on the wind tunnel sidewalls to determine the thrust augmentation. Some thrust augmentation results are reported in Tacina and Fernandez.[1] These dynamic pitot rake and sidewall probes are also used to study the wave physics of the pulsed ejector flow. The dynamic rake and sidewall pressure measurements show a complex pattern of primary and reflected waves with varying wave speeds and wavelengths. "Riding waves" – where one wave is superimposed on a wave of a longer wavelength – are also apparent, especially in the sidewall pressure measurements. This paper will describe a method that can be used to separate these riding waves so that waves originating from different sources may be studied independently.

The pitot probe rake is intended to measure the Mach number. However, to determine the Mach number, the static pressure at the pitot probe location must also be known. However, in this case, using a pitot-static probe that would

*Aerospace Engineer, Inlet Branch, AIAA member
†Aerospace Engineer, Inlet Branch, senior AIAA member
‡Aerospace Engineering Co-op Student, student AIAA member

This material is declared a work of the U.S. Government and is not subject to copyright protection in the United States.

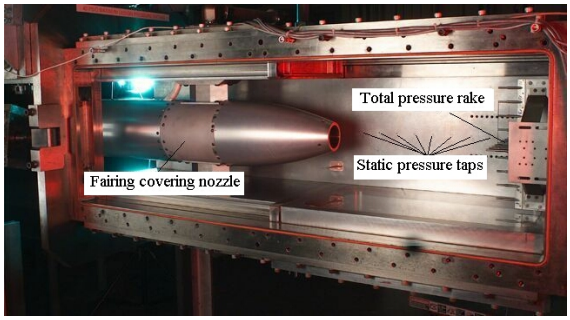

Figure 1: Test section of the NASA Glenn $1' \times 1'$ supersonic wind tunnel with pulsed ejector equipment installed. Shown are the fairing that covers the Mach 3.7 air nozzle and the total pressure rake. Eight of the sidewall static pressure taps are barely visible.

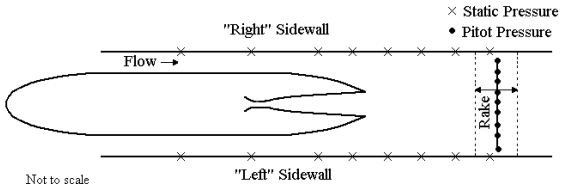

Figure 2: Schematic of experimental setup, showing nozzle, nozzle fairing, location of sidewall pressure taps, and rake location.

accurately measure both the total and the static pressure at a point in supersonic flow was not practical. Customarily, a measured static pressure slightly upstream of the pitot probe is used to determine the Mach number and to correct the pitot pressure for the effect of the bow shock that sits in front of a pitot probe in supersonic flow.[2,3] In unsteady flow, however, using a static pressure upstream of the pitot probe will give incorrect results. In steady flows, shock and expansion waves are usually stationary; however, in unsteady flows there will be shocks and/or expansion waves moving upstream and/or downstream. Therefore, there will be times when a wave traveling downstream will have reached a static pressure tap but not the pitot probe slightly downstream of it, and other times when a wave traveling upstream will have reached the pitot probe but not the static pressure tap. Thus, in a highly unsteady, supersonic flow such as pulsed ejector flow, it is necessary to have some understanding of the wave physics before the Mach number can be accurately determined. This paper develops a procedure for examining the wave physics of an unsteady, supersonic flow.

II. Experimental Setup

In this experiment, a small axisymmetric nozzle (see Figures 1 – 2) placed on the centerline of the NASA Glenn Research Center $1' \times 1'$ supersonic wind tunnel (see Seablom et al[4] for a description of this facility) is pulsed at high frequency using a rotary valve system. The nozzle simulates the primary exhaust flow from a pulse detonation engine (without hot or chemically reacting flow). The wind tunnel test section itself simulates the ejector. Three different nozzles — a Mach 5 air nozzle, a Mach 3.7 air nozzle, and a Mach 4.6 Helium nozzle — are used. The valve system (see Figure 3) is designed to approximate the sharp pressure spikes of a pulse detonation engine. The design of the valve system and nozzles is discussed in Fernandez et al.[5] The wind tunnel itself simulates an ejector with low speed secondary flow; therefore, it is run at Mach numbers of 0.2 – 0.4.

There is mixed subsonic and supersonic flow in this experiment. The flow in the center of the wind tunnel test section downstream of the nozzle is supersonic while the pulse valve is open, but it is subsonic while the pulse valve is closed. In the rest of the test section, the flow is subsonic most of the time.

Four systems are used to take data. A low frequency (1 reading/sec) data recording system records steady state conditions and experimental parameters. The Datamax^{TM} system simultaneously records dynamic data (sample rate:100 kHz) from 41 high frequency Kulite^{TM} pressure transducers placed along the tunnel supply pipes, in static pressure taps on the tunnel walls, and on the pitot rake downstream of the nozzle near the exit of the test section. The Phantom^{TM} high speed (3,6000 to 22,000 frames per second) digital camera records schlieren images that can be adjusted to show density gradients in either the horizontal or vertical directions. Finally, for a few cases, high speed pressure sensitive paint was put on a test section side wall.

Figure 2 shows a schematic of the test section. As shown in this figure, the nozzle fairing intrudes into the wind

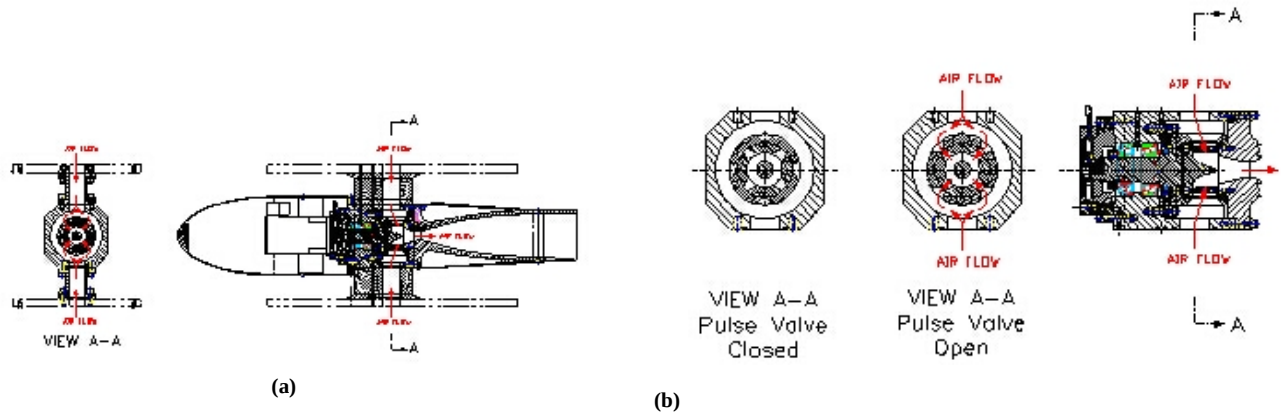

Figure 3: Pulse valve mechanism. Part (a) shows cross sectional views of the pulse valve mechanism, motor, exhaust nozzle and wind tunnel walls, and part (b) shows cross sectional views of the pulse valve mechanism in the closed and opened positions.

Primary flow Mach number	3.7, 4.6, 5
Secondary flow (tunnel) Mach number	0.2, 0.3
Pulse rate (Hz)	0, 30, 60, 80, 100, 120
Duty cycle (%)	8, 11, 16
Pulse strength, defined as pressure fed to pulse valve (psia)	300, 465, 520
Gas for primary flow	air, helium, nitrogen
Gas for secondary flow	air

Table 1: Experimental Parameters

tunnel nozzle block which is directly upstream of the test section. The rectangular test section is 53.25 inches long, 12 inches high, and 12.2 inches wide. The sidewall dynamic pressure taps are at 8.65, 16.65, 24.65, 28.65, 36.65, 40.65, and 44.65 inches downstream of the test section entrance and 6 inches from the bottom of the tunnel. (Throughout this paper, all distances are given relative to the test section entrance.) For most cases, there was also a sidewall dynamic pressure tap at 32.65 inches. The 17-probe pitot rake was cross-shaped, with pitot probes spaced at 1.25 inch increments each arm on the rake. The nozzle exit is at 29.5 inches, and the 17-probe, cross-shaped rake can be moved in one-inch increments from 42.4 to 46.4 inches. At the test section exit, the wind tunnel cross-section changes from rectangular to circular.

The design of pulsed ejectors is a complex problem; many parameters can affect ejector performance. These factors include: Mach number of the primary (nozzle) flow, Mach number of the secondary (ejector) flow, temperature/density ratio of the primary to secondary flow, pulse strength (defined as the pressure entering the pulse valve system), pulse shape, pulse rate, duty cycle (the ratio of pulse duration to cycle duration), ejector to nozzle area ratio, and ejector shape. In this experiment, the pulse rate, pulse strength, duty cycle, Mach number of the primary and secondary flow, ejector to nozzle area ratio, and density ratio were varied (see Table 1).

III. Analysis and Discussion

The purpose of this analysis is to understand the wave physics in supersonic pulsed ejector flow. An accurate knowledge of the corrected total pressure and Mach number at each of the pitot probes on the rake is an important part of this analysis. However, since there is no static pressure measurement at the rake probe locations, some knowledge

of the wave physics of the pulsed ejector is needed to accurately calculate the Mach number at the rake location. (This is discussed in the Appendix.) Therefore, in the rest of this paper, only static and pitot pressure measurements will be discussed.

Ten representative cases were studied. In all cases, the nominal duty cycle was 8%, the nominal secondary flow Mach number was 0.3, and the nominal pulse strength was 465 psia, and the wind tunnel total pressure was 1.9 psia. For five of the cases, the primary flow gas was air, the nozzle exit diameter was 2.41 inches, and the primary flow Mach number was 3.7; for the other five cases, the primary flow gas was helium, the nozzle exit diameter was 2.42 inches, and the primary flow Mach number was 4.6. The pulse frequency varied from 30 to 120 Hz. To minimize the influence of the disturbance caused by the rake, the rake was downstream of the last sidewall static tap for all cases studied in this paper except for Figure 12 in the Appendix. Note that only the left sidewall static probes are examined. This is done because the difference between the pressure taps at two adjacent downstream locations typically dwarfs the difference between the left and right sidewall at the same downstream location. The right sidewall pressure profiles are similar to the left sidewall pressure profiles; if the right sidewall pressures were used instead of the left sidewall pressures in this paper, neither the analysis or the conclusions would change.

A. Type of analysis required

Figure 4 shows that an analysis method that simultaneously gives both time and frequency/scale information is needed. First, however, a preliminary analysis was done in the time domain. For each data set, timing information from the valve system was recorded by the DataMax^{TM} system at the same time as the pressure data. This timing information was used to identify between 22 and 90 (depending on the pulse rate) sets of four pulses for each 3-second reading. These sets of four pulses were then averaged to form an ensemble-averaged pressure. Each part of Figure 4 shows the ensemble-averaged nozzle throat pressure in the top plot, the ensemble-averaged pitot pressure from the center rake probe in the middle plot, and several ensemble-averaged left sidewall pressures in the bottom plot as functions of time. To enable the compression/shock and expansion wave propagation to be seen more clearly, each sidewall pressure is offset by a distance proportional to its distance from the test section entrance. For example: the first sidewall pressure tap is at 8.65 inches and so the first sidewall static pressure is offset by 0.865; the second tap is at 16.65 inches and so the second sidewall static pressure is offset by 1.665; the offsets for the other sidewall static pressures are computed in the same way.

For each case, the nozzle throat pressure plots show four distinct pressure “pulses”. These distinct pressure pulses appear (as expected, at a slightly later time) on each of the center rake pitot pressure plots. However, the rake pitot pressure plots also show smaller pulses superimposed upon the main four pulses. These smaller pulses will be called “riding waves.” Although these riding waves appear in all of the rake pitot pressure plots, they are more pronounced in the cases where the primary gas is air (the plots on the left side of the page) and in the 80 Hz helium case (Figure 4f).

Unlike the rake pitot pressure plots, a pulse directly corresponding to the nozzle pressure pulse cannot be seen on any of the sidewall pressure plots. Instead, in all of the sidewall pressure plots except for the 80 Hz helium case, at least four upstream moving waves with relatively large amplitudes and long wavelengths can be seen. Many shorter-wavelength riding waves are superimposed on these waves. In all of the helium cases except for the 30 Hz case, downstream moving waves with relatively large amplitudes and short wavelengths can be seen on the three sidewall pressure taps that are downstream of the nozzle exit. See, for example, the 120 Hz helium case in Figure 4b. A detailed portion of Figure 4b showing times from 6 ms to 12 ms is shown in Figure 5. In this case, long wavelength upstream moving waves, that start at around 7 ms in the furthest downstream measurement, can be seen at all sidewall pressure tap locations, and large magnitude, short wavelength downstream moving waves can be seen at approximately 9 ms at the three farthest downstream pressure tap locations. The long wavelength upstream moving waves seem to be reflections of the main nozzle pressure pulse caused by the geometry change at the end of the test section. On the other hand, the short wavelength downstream moving waves seen in the last three sidewall pressure plots for most of the helium cases seem to be caused more directly by the flow exiting the nozzle. The origin of the other riding waves seen in the helium sidewall pressure plots, as well as of the riding waves seen in the air sidewall pressure plots and all center rake pitot pressure plots, is unclear.

Studying waves of different wavelengths (and, presumably, different causes) independently requires a data analysis method that separates the original signal into waves of different scale. Since over 300 data sets were collected, to process a major portion of the data, an automated process must be developed. Sections C and D describe two methods (the wavelet transform and Hilbert-Huang transform) that provide time-scale or time-frequency information about a signal, and explain why one method was chosen over the other. However, before that, the next section briefly describes the information obtained from spectral analysis. Note that spectral methods based on the fast Fourier transform work best with linear, stationary signals; wavelet methods work best with stationary or nonstationary linear signals; and that the Hilbert-Huang transform was developed to work with nonlinear, nonstationary data.

B. Spectral analysis

Initially, the frequency content of the rake pitot pressure, nozzle throat, and sidewall static pressure signals was examined using the power spectral density. The curve labeled "FFT" in Figure 6 shows the power spectral density of the centerline rake pitot probe for the 120 Hz helium case shown in Figure 4b. Figure 6a shows the amplitude of the power spectral density using a linear scale and Figure 6b shows it using a logarithmic scale. As expected, the amplitude of the power spectral density is greatest at the nozzle pulse rate of 120 Hz. Not surprisingly, all of the other major components of the power spectral density are harmonics of the nozzle pulse rate. Power spectral densities were computed for the nozzle throat, sidewall static, and rake pitot pressure signals for several other cases. In all cases, the results were similar: the largest power spectral density component occurred at the pulse rate, and all other major components occurred at harmonics of the pulse rate. Since the pulse rate could be effectively controlled in this experiment and so is accurately known before data analysis begins, the power spectral density seems to provide no useful information. However, in other experiments where the pulse rate in not know accurately beforehand, spectral analysis could prove useful.

C. Wavelet Analysis

The continuous wavelet transform was also used to analyze the sidewall pressure profiles. The continuous wavelet transform, defined by

$$\widetilde{p}(t,s) = \frac{1}{\sqrt{s}} \int_{-\infty}^{\infty} p(\tau)\, \psi\left(\frac{\tau - t}{s}\right) dl \tag{1}$$

provides information on both the scales of the features of a signal and the times at which these scales are important.[6–8] Note that in the wavelet transform, the scale s can be thought of as an inverse frequency.

Figure 7a shows the continuous wavelet transform of the static pressure at the farthest downstream (x = 44.65 inches) left sidewall pressure tap for the 120 Hz helium case shown in Figures 4b and 5. A Gaussian wavelet, with $\psi(t) = e^{-t^2/2}$, is used, and the wavelet coefficients, $\widetilde{p}(t,s)$, are computed at 160 scales. White values represent small wavelet transform coefficients; dark values represent large coefficients. To make the variations at all scales easier to see, the color values are set individually at each scale. The pressure signal (rescaled so that it covers the entire figure) is superimposed on the wavelet transform.

Figure 7b plots a small scale wavelet coefficient (scale 100 of 160) as a function of time, and Figure 7c plots the largest scale wavelet coefficient (scale 1 of 160) as a function of time. Note that, although no small scale features are seen in the large scale coefficient plot, relatively large scale features are seen in the small scale coefficient plot. For example, at around 6 ms, a feature with a scale of approximately 2 ms can be seen in the small scale wavelet coefficient plot, and at around 9 ms, a feature with a scale of approximately 0.1 ms can be seen. Although the wavelet transform does at least partially separate the scales of the pressure signal, this separation is not complete. Riding waves can still be seen in the small scale wavelet coefficient plot. Therefore, the continuous wavelet transform is not the ideal way to analyze the pressure signals measured in the pulsed ejector experiment if the true wave physics of the ejector are to be properly categorized.

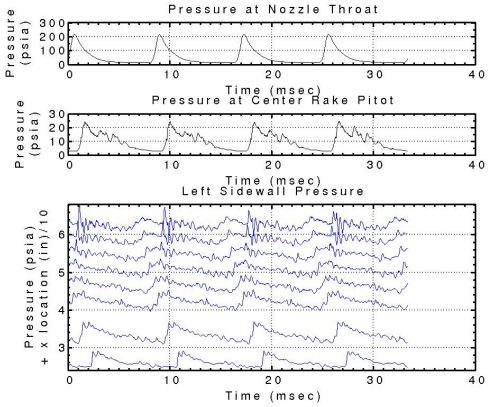

(a) 120 Hz air case

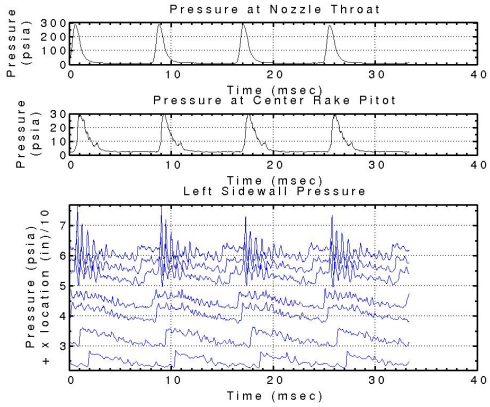

(b) 120 Hz helium case

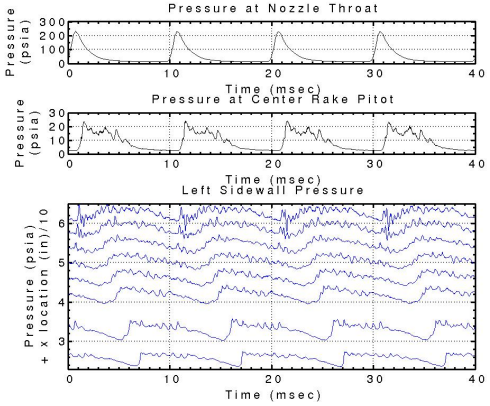

(c) 100 Hz air case

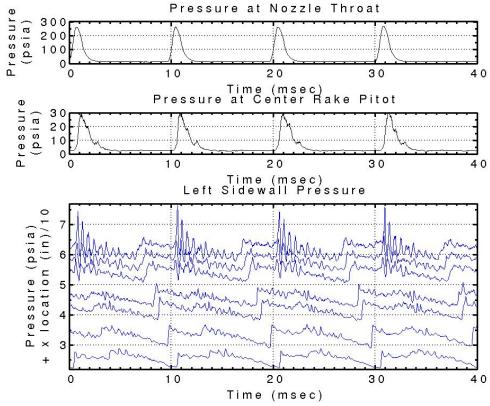

(d) 100 Hz helium case

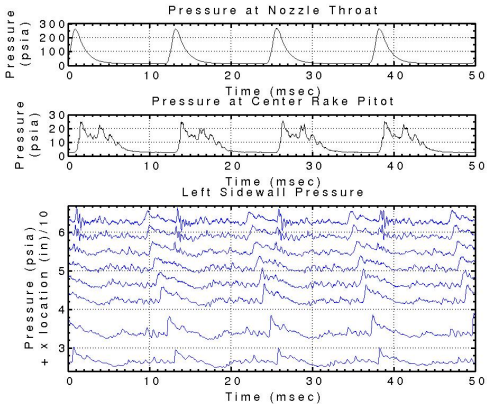

(e) 80 Hz air case

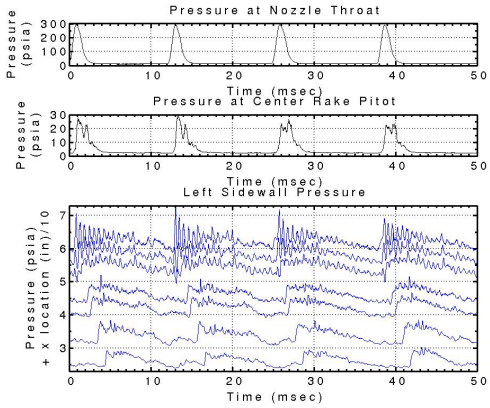

(f) 80 Hz helium case

Figure continued on next page

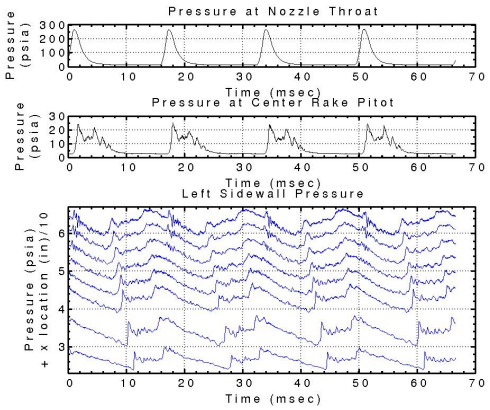

(g) 60 Hz air case

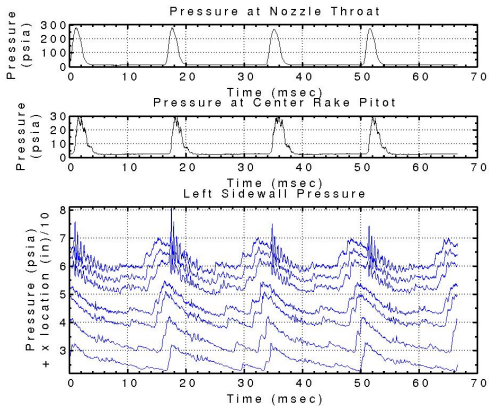

(h) 60 Hz helium case

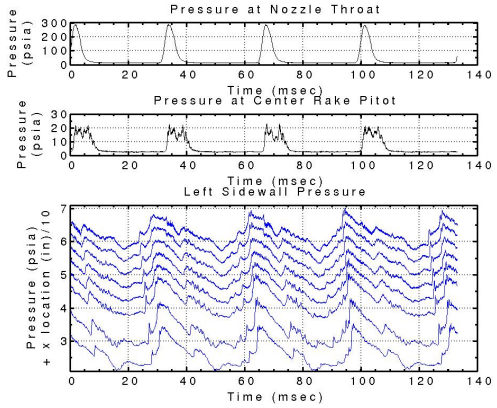

(i) 30 Hz air case

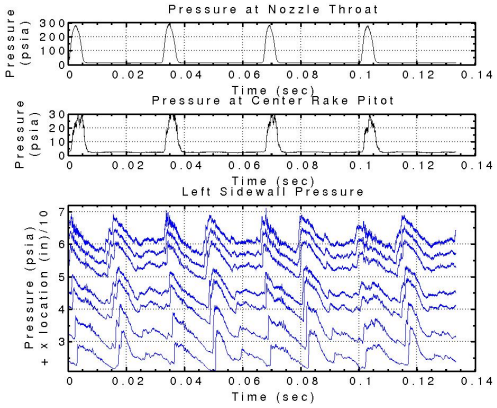

(j) 30 Hz helium case

Figure 4: Nozzle throat, center probe in the pitot rake, and sidewall static pressures as functions of time. To make the plot more clear and to enable the motion of the expansion and compression waves to be seen more clearly, each sidewall static pressure has been offset from the *x*-axis by an amount proportional to its distance from the start of the test section. Parts (a), (c), (e), (g), and (i) show cases with air as the primary gas at pulse rates of 120, 100, 80, 60, and 30 Hz, respectively. Parts (b), (d),(f) (h), and (j) show cases with helium as the primary gas at pulse rates of 120, 100, 80, 60, and 30 Hz, respectively. The primary flow Mach number was 3.7 for the air cases and 4.6 for the helium cases.

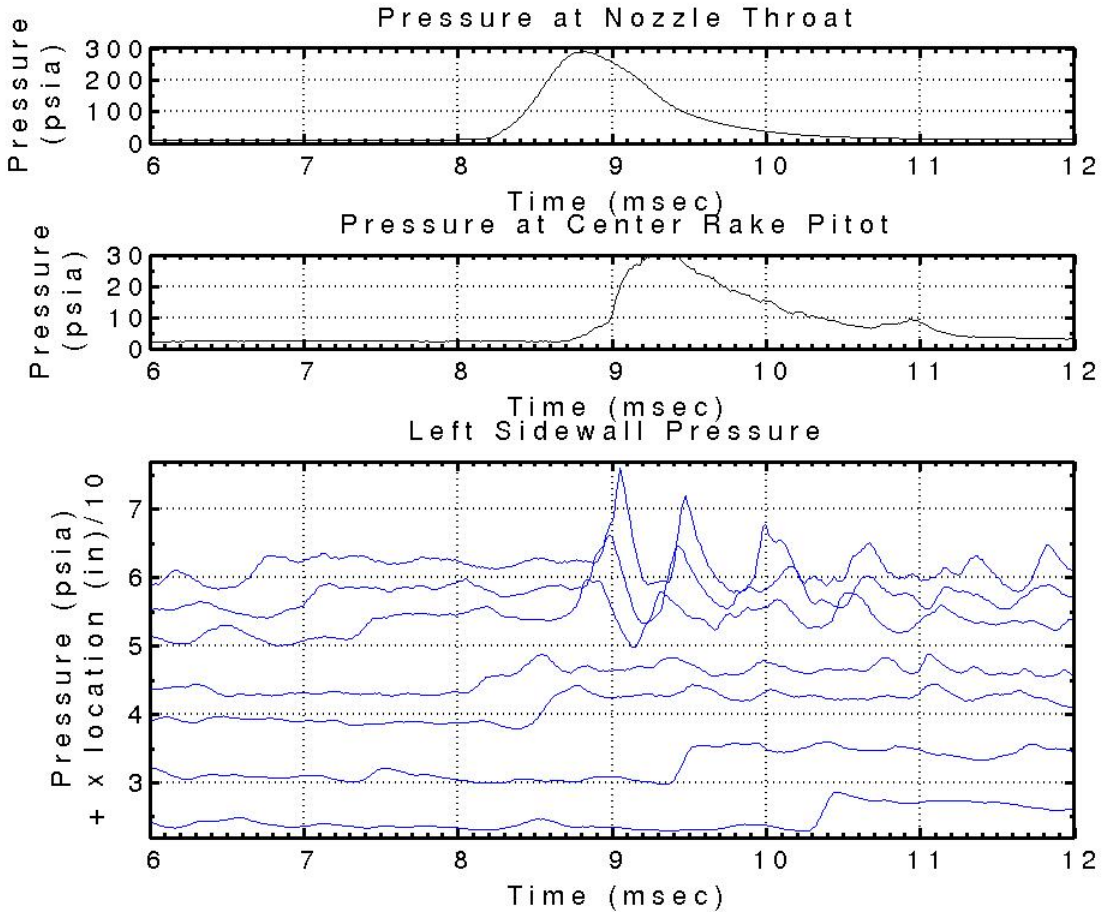

Figure 5: A detailed view of the nozzle throat, center probe in the pitot rake, and sidewall static pressures for the 120 Hz helium case shown in Figure 4b.

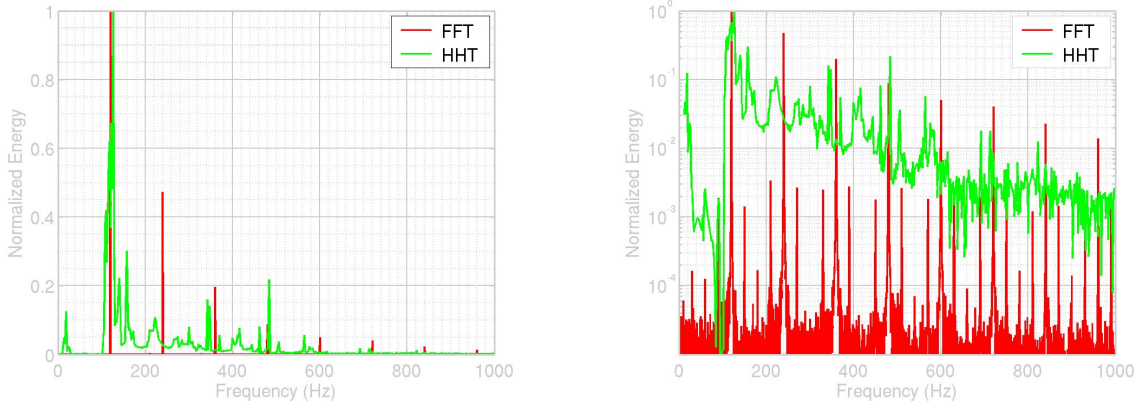

Figure 6: Comparison of the power spectrum computed using the fast Fourier transform (FFT) with the results from the Hilbert-Huang transform (HHT). In part (a), the *y*-axis scale is linear, whereas in part (b) it is logarithmic.

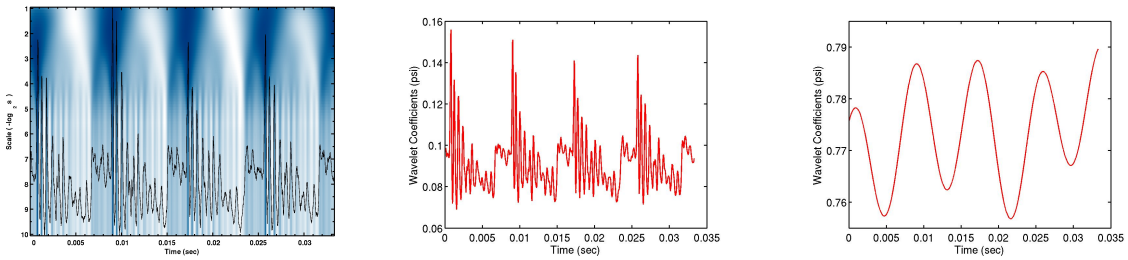

(a) **(b)** **(c)**

Figure 7: (a)Wavelet transform of the farthest downstream left sidewall pressure for the 120 Hz helium case shown in Figure 4b. Plots of (b) small scale (100 of 160) and (c) large scale (1 of 160) wavelet coefficients.

D. Hilbert-Huang transform analysis

The wavelet transform is designed to work with signals that are made up of linear components. A more recent technique, the Hilbert-Huang transform (HHT) has been designed to provide time-frequency information for nonlinear signals.[9–11] HHT analysis is divided into two parts. First, the local maxima and minima of a signal are used to divide the signal into several "intrinsic mode functions" (IMFs). Each IMF has only one mode of oscillation, with no riding waves. If all the IMFs of a signal are added together, the original signal is recovered. Then, the Hilbert transform is performed independently on each IMF. The Hilbert transform can then be used to define the instantaneous frequency. The final result of the HHT is the time-frequency-amplitude representation of the signal. This process is described in detail in Huang et al[9] and in Huang, Shen, and Long.[10]

The HHT was applied to the center rake pitot probe for the 120 Hz helium case shown in Figures 4b and 5. The IMFs that make up this signal are shown in Figure 8a. The HHT of this signal is shown in Figure 8 parts (b) and (c); part (b) shows all the frequency components of the signal, whereas part (c) shows only frequencies less than 2000 Hz. Note that, unlike the small scale coefficients of the wavelet transform, riding waves do not appear in any of the IMF components. Instead, at a given time in each IMF, there appears to be a feature at only one scale, and the scales of all features within a given IMF are similar. (Throughout the rest of this section, these features will be called waves.) Therefore, the HHT will be used to analyze the pressure signals.

Note that the IMFs can separate a pressure signal into physically significant components. This can easily be seen in the IMFs for the farthest downstream left sidewall static pressure for the same case, which are shown in Figure 9. The left sidewall pressure plots shown in Figures 4b and 5 clearly show short wavelength, large amplitude, downstream moving waves at approximately 9 ms and longer wavelength, smaller amplitude upstream moving waves at approximately 7 ms (see the discussion in subsection A). Comparing the IMFs with Figure 4b shows that the fourth IMF from the top of Figure 9 contains waves that start at the same time and have the same wavelength and amplitude as the downstream moving waves in Figure 4b. This comparison also shows that the eighth IMF from the top of Figure 9 have roughly the same magnitude and the same frequency (1 per nozzle pulse, or 120 Hz) as the the upstream moving waves.

To understand the wave physics of the pulsed ejector, it is necessary to separate the waves so that the waves caused by different physical phenomena can be studied independently. As mentioned in subsection A, the short wavelength downstream moving waves seen in the fourth IMF of Figure 9 seem to be directly attributable to the flow exiting the nozzle. However, a comparison of wavelength and timing of these downstream moving waves with the pressure pulses seen in the nozzle and center rake pitot portions of Figures 4b and 5 (that are obviously caused by the nozzle exhaust) show that the short wavelength, downstream moving waves in the sidewall portion of Figure 4b are not the nozzle exhaust itself. Schlieren images confirm that the jet issuing from the nozzle has not impinged on the tunnel sidewalls. One possible cause of the short wavelength, large amplitude, downstream moving pressure pulses seen in the sidewall pressure plots is starting vortices of the jet issuing from the nozzle. Previous work has shown that the interaction of these starting vortices with the ejector sidewalls is a major factor in ejector performance.[12] To more conclusively determine the origin of these downstream moving pulses, it is necessary to contrast these waves between the three

farthest downstream sidewall pressure taps for cases at different pulse rates and duty cycles. This is extremely difficult to do when these waves are superimposed upon waves of different frequency and magnitude, as is seen in the original pressure plot in 4b. Thus, a technique like the HHT is needed to study these waves effectively.

The long wavelength upstream moving waves seen in the eighth IMF seem to be reflections of the main nozzle pressure pulse. These reflections are most likely to occur at the test section exit where the geometry changes from rectangular to cylindrical. However, to more definitively determine the source of these reflections, it is necessary to compare the long wavelength waves at several sidewall taps for cases of varying pulse rates and duty cycles. When many riding waves with shorter wavelengths are superimposed on these long wavelength upstream moving waves, it is almost impossible to make good quantitative comparisons. A technique like the HHT must be used. In some cases, the IMFs may have to be found before these long wavelength upstream moving waves can be seen at all. An example of this is the 80 Hz helium case shown in Figure 4f; here, the long wavelength upstream moving waves cannot be definitively identified at the three farthest downstream sidewall pressure taps measurements because the short wavelength downstream moving waves appear to reach these pressure taps at approximately the same time. In this case, the IMFs are needed to clearly identify the large wavelength upstream moving waves. If pulse detonation engines are used in enclosed environments such as in a gas turbine engine, techniques such as the one being developed will be needed to effectively understand and quantify the flow phenomena affecting engine performance.

IV. Summary

The 1-foot by 1-foot supersonic wind tunnel at NASA Glenn Research Center was used to simulate a supersonic pulsed ejector. A nozzle mounted in the wind tunnel was used to simulate high speed primary flow, while the tunnel itself simulated an ejector with low speed secondary flow. The primary Mach number, secondary Mach number, duty cycle, pulse rate, primary flow gas, and the location where the thrust augmentation was measured were varied. Dynamic pressure sensors were placed at the nozzle throat, in static taps in the wind tunnel sidewalls, and on a cross-shaped, 17-probe pitot rake. These dynamic pressure signals were analyzed and it was found that:

- The rake probe pitot pressures and the sidewall pressures show many pressure “pulses” of different wavelengths and amplitudes superimposed upon each other. These pulses are called “riding waves.”
- Spectral analysis using the fast Fourier transform accurately determines the pulse rate, but does not yield any other useful results for the cases studied here.
- To separate the effects of pulses at different scales, two time-frequency or time-scale analysis methods were considered: the continuous wavelet transform and the Hilbert-Huang transform (HHT).
- The continuous wavelet transform did partially separate the pressure pulses at different scales, but did not eliminate the riding waves.
- The Hilbert-Huang transform successfully separated the signal into different components,called Intrinsic Mode Functions (IMFs). Each IMF contained pressure pulses of roughly the same frequency, and no significant riding waves were observed. The IMFs were found to be physically meaningful.
- Thus, the HHT was chosen as a method to automate data analysis. With readings taken at more than 400 experimental conditions, an automated technique with minimal human intervention is being developed to process all of the experimental data
- The presence of these riding waves in the original pressure signals makes it difficult to determine the Mach number from a pitot probe because the reference static pressure is at a different location. Thus, some understanding of the wave physics of the pulsed ejector is needed before the Mach number at the rake can be calculated accurately.
- If possible, future experiments involving supersonic, highly unsteady flow should determine the Mach number using a pitot-static probe specifically developed for this type of flow[3] instead of a pitot probe that relies on a separate static pressure measurement taken at a different location.

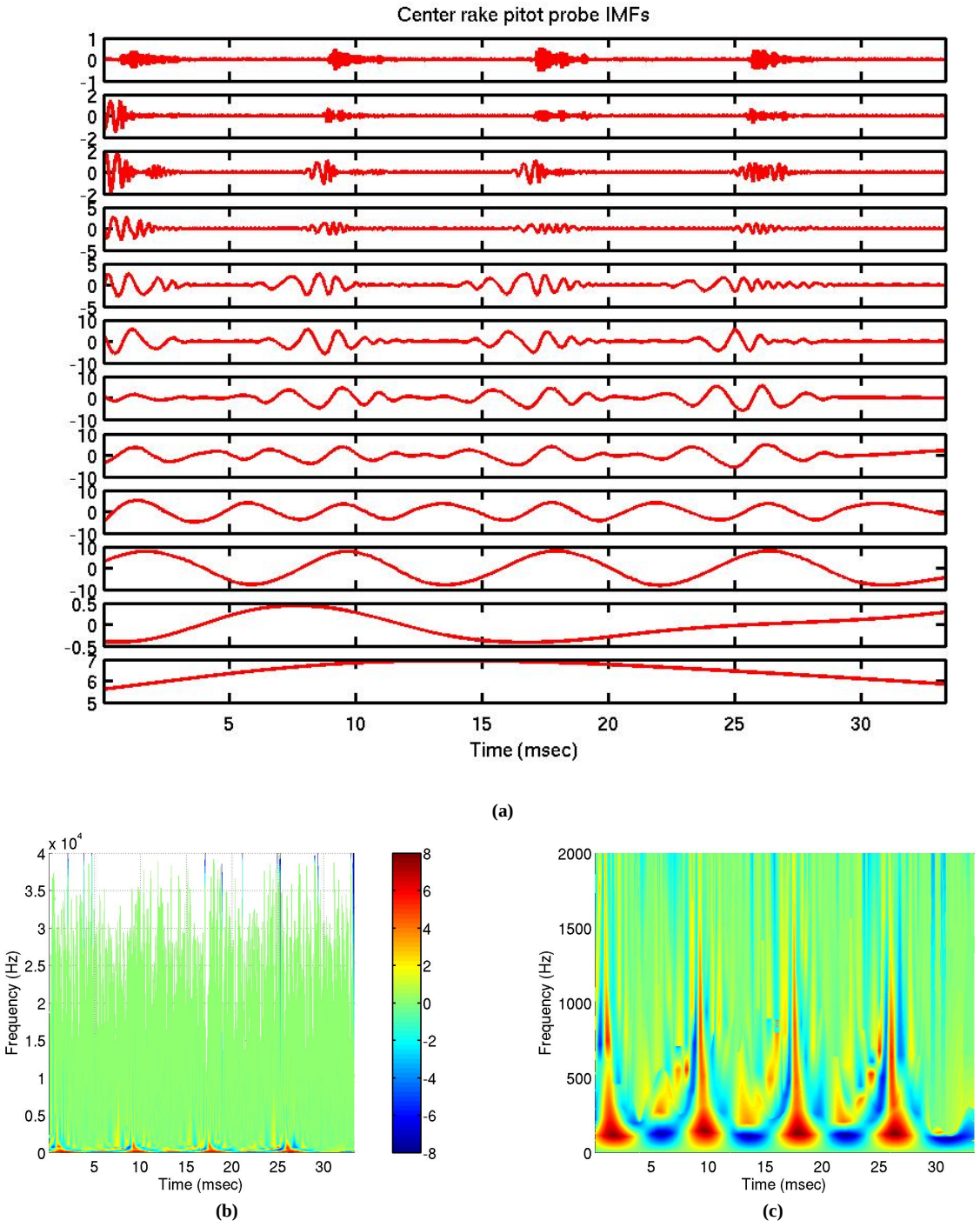

Figure 8: For the center rake pitot pressure for the 120 Hz helium case, part (a) shows the intrinsic mode functions and parts (b) and (c) show the Hilbert-Huang transform.

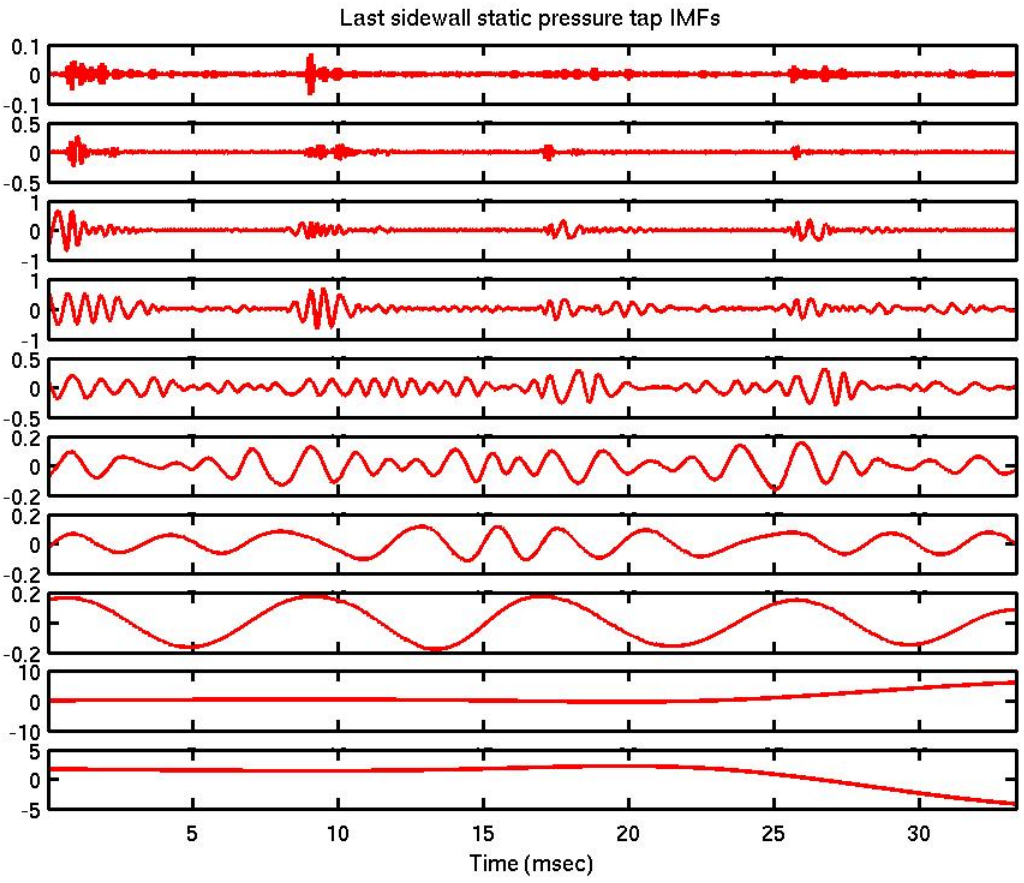

Figure 9: IMF for the farthest downstream left sidewall static pressure tap for the 120 Hz helium case.

References

[1]Tacina, K. M., Fernandez, R., and Moody, S. M., "Thrust augmentation in an unsteady supersonic pulsed ejector," AIAA–2004–0866, 2004.

[2]Blake, W. K., "Differential Pressure Measurement," *Fluid Mechanics Measurements*, 1983, pp. 61–95.

[3]Porro, A. R., "Pressure Probe Designs for Dynamic Pressure Measurements in a Supersonic Flow Field," NASA/TM–2001-211096, July 2001.

[4]Seablom, K. D., Soeder, R. H., Stark, D. E., Leone, J. F., and Henry, M. W., "NASA Glenn 1- by 1-Foot Supersonic Wind Tunnel User Manual," NASA/TM–1999-208478, 1999.

[5]Fernandez, R. Slater, J. and Paxson, D., "Pulsed Ejector Wave Propagation Test Program," *Confined Detonations and Pulse Detonation Engines*, 2003, pp. 303–326.

[6]Farge, M., "Wavelet Transforms and Their Applications to Turbulence," *Annual Review of Fluid Mechanics*, Vol. 24, January 1992, pp. 395–458.

[7]Mallat, S., *A Wavelet Tour of Signal Processing*, 1999.

[8]Kaiser, G., *A Friendly Guide to Wavelets*, 1994.

[9]Huang, N. E., Shen, Z., Long, S. R., Wu, M. C., Shih, H. H., Zheng, Q., Yen, N.-C., Tung, C. C., and Liu, H. H., "The empirical moed decomposition and the Hilbert spectrum for nonlinear and non-stationary time series analysis," *Proceedings of the Royal Society of London*, Vol. 454, 1998, pp. 903–995.

[10]Huang, N. E., Shen, Z., and Long, S. R., "A new view of nonlinear water waves: the Hilbert spectrum," *Annual Review of Fluid Mechanics*, Vol. 31, 1999, pp. 417–457.

[11]Huang, N. E., Wu, Man-Li C.and Long, S. R., Shen, S. S. P., Qu, W., Gloersen, P., and Fan, K. L., "A confidence limit for the empirical mode decomposition and Hilbert spectral analysis," *Proceedings of the Royal Society of London*, Vol. 459, 2003, pp. 2317–2345.

[12]Wilson, J., "A Simple Model of Pulsed Ejector Thrust Augmentation," NASA/CR–2003-212541, 2003.

Appendix

Need for further analysis: Mach number

The purpose of this analysis is to understand the wave physics in supersonic pulsed ejector flow. An accurate knowledge of the corrected total pressure and Mach number at each of the pitot probes on the rake is an important part of this analysis. However, before deciding that some knowledge of the wave physics is needed to determine the corrected total pressure and Mach number at the rake, the first question that needs to be asked is: would the error level in a first-order analysis be acceptable? Would using the static pressure from the tap just upstream or downstream of the rake, or using a pressure linearly interpolated based on these static pressure taps, be likely to yield accurate results?

In order to determine if a first-order analysis would be acceptable, it is necessary to know (1) the uncertainty in the static pressure resulting from using a first-order analysis on the highly dynamic pressure signals recorded in these experiments and (2) the effect this uncertainty would have on the data analysis.

To estimate the difference between the static pressure at the sidewall and the (unmeasured) true static pressure at the rake, the pressure difference between consecutive sidewall static pressure taps was examined. For all cases, the axial rake location is either between that of the two last static taps or is downstream of the last static tap. Furthermore, there is no geometry variation in this part of the wind tunnel. A common assumption made in wind tunnel testing is that the static pressure is constant in the direction normal to the tunnel flow. Using this assumption, the difference in pressure between the last two static pressure taps should be of the same order of magnitude as the difference in static pressure between the rake and the nearest static tap.

For each of the ten cases shown in Figure 4, Figure 10 shows the percentage of time when the last two static taps on the left sidewall differed by a certain amount. Part (a) shows the five air cases, and part (b) shows the five helium cases. For all of the air cases, the last two sidewall pressures are within 10% of each other more than 90% of the time. The percentage of time that the difference between the last two left sidewall static pressures is large is greater for the helium case, but the last two sidewall pressures are still within 10% of each other almost 80% of the time. However, for both the air and helium cases, the percentage of time that the pressure differences are large increases with increasing pulse rate. In the 120 Hz helium case, the difference between the last two static pressures on the left sidewall is greater than 20% for almost 10% of the time.

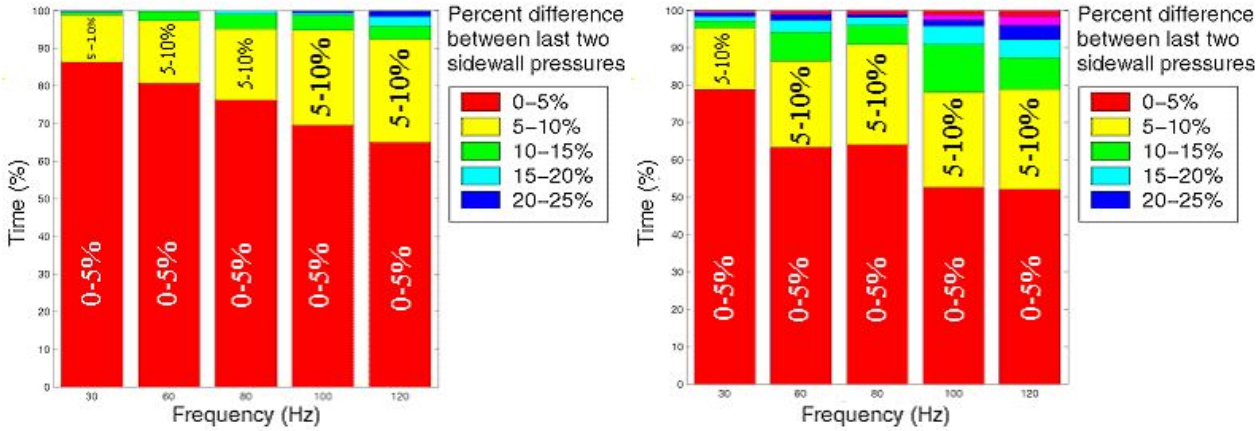

Figure 10: Percentage of time that the last 2 sidewall pressures differ by a given percentage at various frequencies. Shown are (a) air and (b) helium cases.

The error in the Mach number, σ_M, due to the error in static pressure, σ_{p_s}, is given by

$$\sigma_M = \sigma_{p_s} \frac{\partial M}{\partial p_s} \tag{2}$$

where

$$\frac{\partial M}{\partial p_s} = \begin{cases} -\frac{1+\frac{\gamma-1}{2}M^2}{\gamma p_s M} & \text{if } M \leq 1, \\ -\frac{M\left(2\gamma M^2-\gamma+1\right)}{2\gamma p_s\left(2M^2-1\right)} & \text{if } M > 1. \end{cases} \tag{3}$$

Figure 11a shows the derivative of Mach number, M, with respect to static pressure, p_s. To estimate the uncertainty in Mach number caused by using static pressure taps at downstream locations that are different than the downstream location of the pitot measurements, a typical centerline Mach number of 2 and a typical static pressure of 1.8 psi were used. At a typical static pressure uncertainty of 5% (0.09 psi), the uncertainty in Mach number caused by the uncertainty in static pressure is 0.05 (2.5%). However, at the same conditions but with a high uncertainty in static pressure (20%, or 0.36 psi), the uncertainty in Mach number is 0.2 (10%).

The difference between the two last sidewall static pressure taps can also make it difficult to determine if there is reverse flow. Measuring a pitot pressure that is lower than the static pressure usually means the flow is either reversed or that the angle between the flow direction and the pitot probe is high. However, in unsteady, subsonic flow where the pitot pressure is less than the static pressure downstream of it and greater than the static pressure upstream of it (or vice versa), it is unclear whether reverse flow is occurring or a compression wave has reached one static tap but not the pitot probe and the other static tap. Figure 12 shows the last two left static pressures and the nearest rake pitot probe pressure as functions of time. The case shown is identical to the 120 Hz air case show in Figure 10a except that the rake location is between the two pressure taps. As Figure 12 shows, the nearest rake pitot probe pressure is below one static pressure but higher than the other for a significant percentage of the time. At some time — for example, at 5.7 ms — seems to be due to the moving expansion and compression waves, not reverse flow. At other times — for example, at 6.5 ms — it is unclear whether reverse flow is occurring.

These results indicate that using linearly interpolated or extrapolated static pressures to estimate the static pressure at the rake pitot probe location may yield inaccurate Mach numbers. The results shown in the Figures 13 and 4 verify this. Figure 13 compares the measured sidewall static pressures at 40.65 and 44.65 inches with the sidewall static pressure at 42.65 inches found by linear interpolation and 46.65 inches found by linear extrapolation for the 120

Hz Mach 3.7 air case (see also Figure 4a). Note that both the interpolated and extrapolated signals are qualitatively different than either of the two measured pressure signals. See, for example, times 1 ms and 9.4 ms in Figure 13a and 13b. Note also that the maximums and minimums of the interpolated signal in Figure 13a are less extreme than those of the measured pressures, and that those of the extrapolated signal in Figure 13b are more extreme than those of the measured pressures. These results, along with Figure 4, show that a simple spatial interpolation or extrapolation to find the pressure at an intermediate location may not give very accurate results when the nozzle pulse rate is high.

Figure 14 shows results from initial time accurate axisymmetric computational fluid dynamics (CFD) calculations. The geometry used for these CFD calculations was similar to the experimental setup, but the nozzle Mach number was slightly different and the tunnel test section geometry was axisymmetric. The nozzle pressures used were similar to those used in a 30 Hz pulse rate case. Figure 14a compares the CFD centerline static pressure at 43.35 inches (a typical rake location in the experiment) with the value found by linear interpolation using the CFD sidewall pressures at 40.65 inches and 44.65 inches (the locations of the last two sidewall static pressure taps in the experiment). This figure shows that the correct static pressure can differ by that found using linear interpolation by more than 50%. Figure 14b compares the CFD Mach number at the same location with that found using the CFD pitot pressure and the interpolated static pressure from Figure 14a; the Mach numbers can differ by more than 30%.

These results show that some understanding of the wave physics of the pulsed ejector is needed to accurately find the Mach number at the rake location. The next question is: do the wave physics of the pulsed ejector need to be understood to accurately calculate the thrust at the rake location? To determine this, the error in the instantaneous thrust, σ_T, (where the instantaneous thrust T is $T = \int_A \gamma p_s M^2 dA$) due to the error in the static pressure, which is given by

$$\sigma_T = \sigma_{p_s} \frac{\partial T}{\partial p_s} \tag{4}$$

where

$$\frac{\partial T}{\partial p_s} = \frac{\partial T}{\partial p_s} + 2M \frac{\partial T}{\partial M} \frac{\partial M}{\partial p_s} = \begin{cases} M^2 - 2 & \text{if } M \le 1, \\ \frac{M^2}{1-2M^2} & \text{if } M > 1. \end{cases} \tag{5}$$

is graphed in Figure 11b. This figure shows that the uncertainty in the static pressure is less important in accurately determining the thrust than it is in accurately determining the Mach number. Since σ_{p_s} is less than 10% most of the time in all cases, σ_T should also be small; at supersonic Mach numbers, if σ_{p_s} is less than 10%, σ_T will be less than 5%. In addition, it is the time-averaged thrust that is of interest, not the instantaneous thrust, so larger σ_T for a very small percentage of the time should not have too large an impact on the overall uncertainty in the thrust. Thus, although an understanding of the wave physics of the pulsed ejector is necessary to determine the instantaneous Mach number at the rake location, it is not as critical when using the pitot rake to determine the thrust at the ejector location.

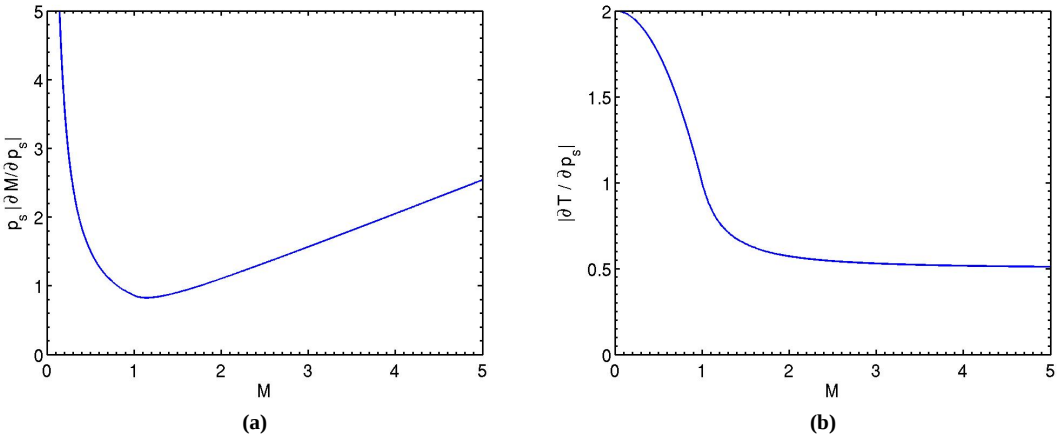

Figure 11: (a) Static pressure times the absolute value of the derivative of Mach number with respect to static pressure, $p_s \left|\frac{\partial M}{\partial p_s}\right|$. (b) The derivative of instantaneous thrust with respect to static pressure.

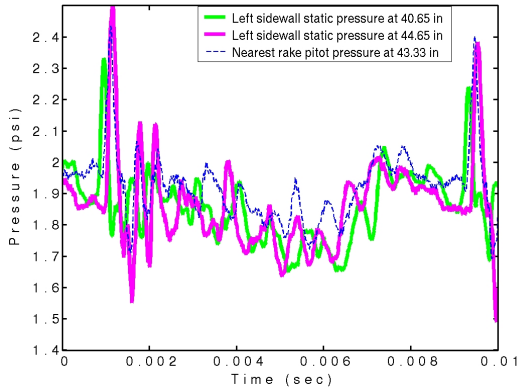

Figure 12: Comparison of the last two sidewall static pressure taps with the nearest rake pitot pressure for the 120 Hz air case similar to the one shown in Figure 10a.

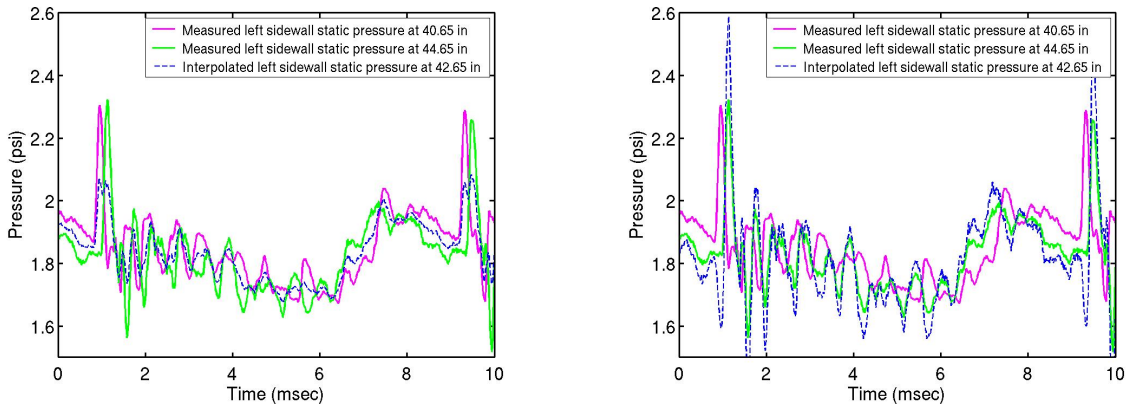

Figure 13: Measured left sidewall static pressures at 40.65 and 44.65 inches compared with the left sidewall static pressure at (a) 42.65 inches found by linear interpolation and (b) 46.65 inches found by linear extrapolation.

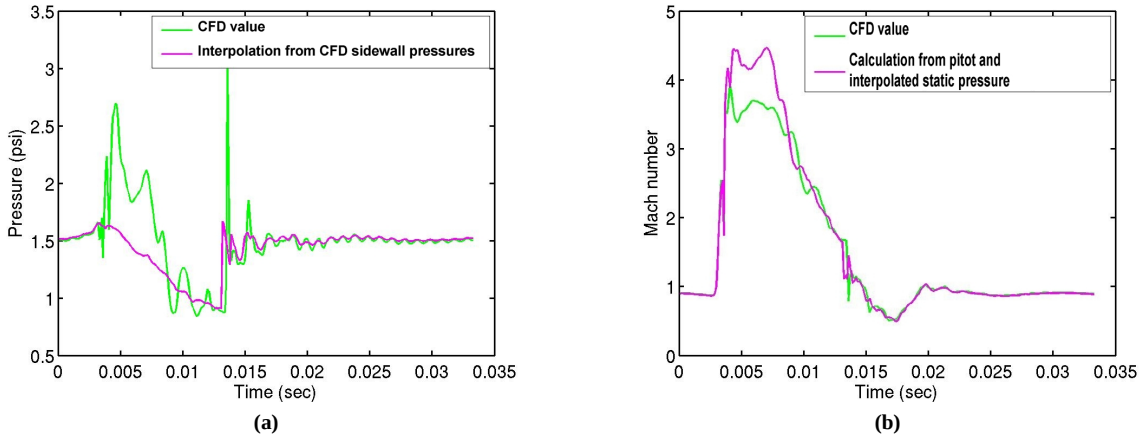

Figure 14: Comparison of (a) the CFD centerline static pressure at 43.35 inches with value found using linear interpolation with the CFD sidewall static pressures and (b) the CFD Mach number at 43.35 inches with that calculated using the pitot pressure and the interpolated static pressure from part (a).